A multidomain 0D model for continuous positive airway pressure ventilation circuit design: Validation and applications

A Multidomain 0D Model for Continuous Positive Airway Pressure Ventilation Circuit Design: Validation and Applications

Andrea Formaggio[a,b,*], Margherita De Luca[a,b], Simone Borrelli[a,b], Giovanni Putame[a,b], Nello De Vita[c,d], Fabio Minelli[d], Francesco Della Corte[c], Rosanna Vaschetto[c], Alberto L. Audenino[a,b], Carlo Olivieri[e], Mara Terzini[a,b]

[a] Department of Mechanical and Aerospace Engineering, Politecnico di Torino, Turin, Italy
[b] Polito[BIO]Med Lab, Politecnico di Torino, Turin, Italy
[c] Department of Translational Medicine, Università del Piemonte Orientale, Novara, Italy
[d] Anesthesia and Intensive Care, Azienda Ospedaliero-Universitaria Maggiore Della Carità, Novara, Italy
[e] Anesthesia and Intensive Care, Sant'Andrea Hospital, ASL VC, Vercelli, Italy

* Corresponding author at: Corso Duca degli Abruzzi, 24, 10129 Torino, Italy. E-mail address: andrea.formaggio@polito.it

Abstract

This study focuses on optimizing a non-invasive ventilation (NIV) circuit for the treatment of hypoxemic respiratory failure using continuous positive airway pressure (CPAP). A multidomain 0D *in silico* approach was employed, creating a lumped circuit model of an innovative NIV-CPAP system in Mathworks® Simulink. The model relies on *in vitro* tests on commercial components characterizing pneumatic resistive behavior, and it exploits an extended resistance-inductance-capacitance model for the patient's respiratory system, recurring to sigmoidal pressure-volume behavior characteristic of pathological conditions. The NIV-CPAP system was assembled *in vitro* and connected to a lung simulator to validate the model under healthy and pathological conditions (acute respiratory distress syndrome and chronic obstructive pulmonary disease). The study explored the impact of key features on the ventilation circuit, such as interface leakage, air volume within the circuit, and resistance induced by circuit components.

Validation of the 0D model through in vitro tests showed correlation coefficients between 0.9 and 1. Interface leakage caused reductions of up to 6% in delivered static pressure. Changes in air volume (mask or helmet interface, reservoirs adding) resulted in a maximum 8% decrease in pressure oscillations. Increased resistances from the starting ventilation circuit produced a tidal volume reduction of less than 1%. An optimized configuration that balanced resistances between limbs improved intrinsic positive end-expiratory pressure generation.

The proposed 0D model proved to be effective in guiding the design of the innovative device, providing computational efficiency and flexibility; it demonstrated its reliability as a tool to support the optimization of non-invasive ventilation circuits.

Keywords: 0D model, closed breathing circuit, continuous positive airway pressure, MATLAB/Simulink, non-invasive ventilation

Mechanical ventilation (MV), invasive mechanical ventilation (IMV), non-invasive ventilation (NIV), Continuous Positive Airway Pressure (CPAP), positive end-expiratory pressure (PEEP), intrinsic positive end-expiratory pressure (PEEPi), funtional residual capacity (FRC), acute respiratory distress syndrome (ARDS), Chronic Obstructive Pulmonary Disease (COPD), resistance-inductance-capacitance (RIC), predicted body weight (PBW),

1 Introduction

Mechanical ventilation (MV) constitutes a therapeutic approach wherein a mechanical ventilator supports patients with severe respiratory failure, allowing them to ventilate adequately and to maintain normal gas exchange between the lungs and the environment [1]. MV does not cure lung tract diseases, but it allows the body to recuperate from the syndrome responsible for respiratory failure by providing adequate oxygenation and by removing carbon dioxide. Indications for establishing mechanical ventilation are refractory hypoxemia, ventilatory failure, shock with metabolic acidosis, and airway failure due to altered mental status or physical obstruction [2,3]. MV can be delivered in two distinct forms: invasive mechanical ventilation (IMV) and non-invasive ventilation (NIV). In the case of IMV, an endotracheal tube, nasotracheal tube, or tracheostomy cannula are used to carry out the ventilation. On the other hand, NIV employs interfaces such as a facial mask, mouthpiece, or helmet, which do not require endotracheal tube placement. The implementation of non-invasive oxygenation strategies helps preserve the natural airway protection mechanisms, such as the ability to cough and clear secretions. Additionally, it avoids the potential complications associated with endotracheal intubation, which encompass laryngeal and tracheal trauma, as well as the issues related to IMV which include ventilator-induced lung injury, ventilator-associated pneumonia, mucosal ulceration, respiratory muscle wasting, and swallowing dysfunction, diaphragm dysfunction and atrophy [4–9]. Despite this, NIV is not free from drawbacks such as the development of skin pressure sores, the risk of malnutrition especially in patients with the need for prolonged NIV and the risk of self-inflicted lung injury in patients with excessive respiratory effort and work of breathing [10].

MV can be delivered in two primary modes: controlled ventilation and assisted ventilation. In controlled modes, the ventilator entirely takes over the role of the respiratory muscles, and the target variable controlled by the ventilator can be either the volume or the pressure. In assisted modes, the ventilator provides support to the patient's respiratory efforts. In spontaneously breathing patients it is possible to apply a continuous positive pressure into the lungs delivering the so-called CPAP (Continuous Positive Airway Pressure) therapy in NIV modality. CPAP does not provide inspiratory support but maintains positive airway pressure at end-expiration [11]. The delivered positive pressure increases the patient’s functional residual capacity (FRC), opens under-ventilated alveoli, decreases atelectasis, and improves lung compliance [12]. Due to these advantages, CPAP therapy is employed in the treatment of different kinds of hypoxemic respiratory failure. This condition was notably prevalent during COVID-19 pandemic, where a significant number of patients exhibited symptoms that gradually led to progressive hypoxemic respiratory failure [13]. One such case was the occurrence of acute respiratory distress syndrome (ARDS), where the inflammatory lung condition leads to leakage of fluid into the lung spaces resulting in hypoxemia. The efficacy of non-invasive ventilation delivered through a continuous positive airway pressure (NIV-CPAP) as a supportive treatment for ARDS varies based both on the severity of the pathology (most successful in patients with mild ARDS [14], and mild-to-moderate ARDS secondary to SARS-CoV-2 [15]) and possibly on the disease type (“L” and “H” phenotypes) [16].

At present, NIV-CPAP is commonly administered through an open-configuration ventilation circuit, typically using masks or helmet interfaces, which show better patient tolerance in clinical practice compared to masks [17]. In these systems, a voluntary leak is generated at the interface, which controls the constant positive pressure and the washout flow of exhaled gases in two ways: (1) by generating the flow through the device (e.g., Venturi flowmeter) and regulating pressure via a PEEP valve that adjusts the leak, and (2) by controlling the pressure generated by the device (typically via a turbine) and managing the flow through an exit port at the interface. These systems have several disadvantages: high oxygen consumption to achieve therapeutic concentrations, dependence on the hospital’s high-pressure gas lines, elevated noise levels, aerosolization of pathogens, as could have happened during COVID-19, and the need for a humidification system. To minimize these drawbacks, an innovative ventilation system that operates in a

closed-loop circuit, and inspired by anaesthesia systems, was previously proposed and preliminarily tested on a healthy subject [18,19]. However, conducting experiments on mechanical ventilators is not only expensive but also could be dangerous for the patients. In this context, multidomain 0D *in silico* models can provide significant contribution in evaluating innovative ventilation mode and support the development of mechanical ventilation devices. These mathematical methods represent different physical domains (such as mechanics, electricity, fluid dynamics, etc.) in a system, where each part is treated as if it were a point without dimensions. Each pointwise element of the circuit is therefore described by spatially averaged values (0D) and physical variables that change only over time. The advantage is thus to simulate the interaction of the various parts of the system on a global level with very low computational cost.

This approach has been employed in several studies, in order to understand the interaction between mechanical ventilators and human lungs [20–26]. Previous studies focused on IMV, while scant attention was dedicated to NIV-CPAP mode. Since pathological patients undergoing CPAP therapy can manifest varying deformations across different regions of the pressure-volume curve, showing a non-linear sigmoidal behaviour, the present study introduces a novel non-linear patient model based on the extended linear resistance-inductance-capacitance (RIC) model present in literature [27–30]. Additionally, this work introduces, for the first time, an *in silico* investigation of spontaneous breathing in ventilation circuits using a 0D modelling approach.

The goal is to develop a validated multidomain 0D *in silico* approach to optimize the non-invasive closed-loop ventilation circuit proposed by Cavaglià et al. [18], by investigating the potential effects of the design choices of the circuit on the administered treatment across a variety of patients.

2 Materials and Methods

The novel NIV-CPAP closed circuit proposed in [18] can be implemented using existing components from the traditional NIV-CPAP open-loop configuration. Figure 1 illustrates the pneumatic scheme of the system. Once the air passes through a filter (1) to eliminate impurities, it is pressurized by a blower (2). A second inlet is designated for the oxygen supply, allowing for potential enrichment of the breathing air using an O_2 source (3), like a tank or an oxygen concentrator. The oxygen enters the circuit via the O_2 directional proportional valve (4), which works as a metering valve by regulating the degree of its opening. The mixture of air and oxygen is delivered to the patient through the inspiratory limb, which includes an antiviral filter (5), a balloon as a reservoir (6) and a check valve (7) to ensure unidirectional flow. The gas is directed into the interface (8), which administers CPAP therapy to the patient. The interface (8) inevitably introduces an air leakage into the surrounding environment (9). Symmetrically, a check valve (10), a reservoir (12) and an antiviral filter (13) are placed in the expiratory limb. In addition, the soda lime (11) is used as a CO_2 absorber to purify the exhalation avoiding CO_2-rebreathing. The gas analysis unit includes a set of sensors that monitor various ventilation-related parameters. The rotational speed of the blower is regulated to maintain the pressure at the desired therapeutic level, as measured by the pressure sensor (15). An O_2 sensor (16) monitors the oxygen concentration, which is used to control the opening degree of the inlet metering valve. To ensure patient safety, a CO_2 sensor (17) monitors the carbon dioxide concentration. Finally, a safety three-way valve (14) is actuated to open the circuit when the pressure sensor or the CO_2 sensor detects abnormal and potentially harmful levels for the patient. The ventilation system was designed with disposable components (outside the “device” box) and components housed within the ventilator casing (inside the “device” box). Specifically, antiviral filters are placed at the connections of the device limbs to prevent contamination of the device itself.

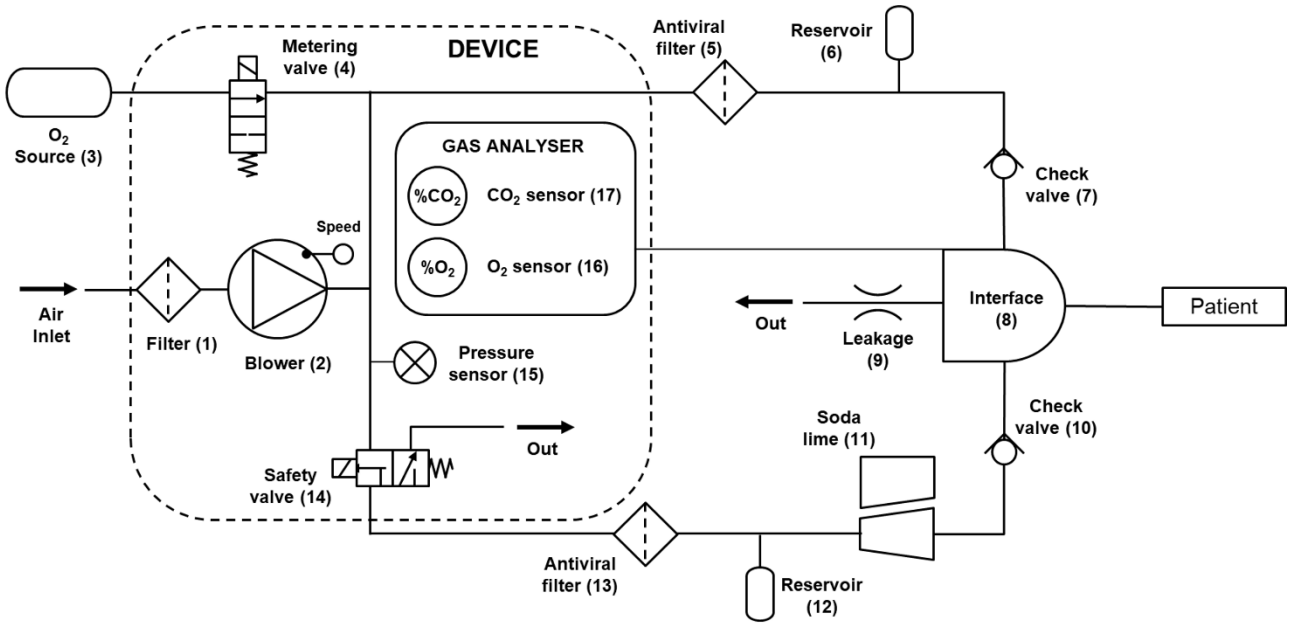

Figure 1. Pneumatic scheme of the ventilation circuit with ISO symbols.

2.1 Equation of motion of the respiratory system

In respiratory mechanics, at any time (t), the airways pressure P_{aw} is equal to the sum of three pressures according to Eq. (1): the alveolar pressure at the beginning of the inspiration (P_0) which can be the atmospheric pressure or a positive end-expiratory pressure (PEEP), the resistive pressure (P_{res}) and the elastic pressure (P_{el}).

$$P_{aw}(t) = P_0 + P_{res}(t) + P_{el}(t) \quad (1)$$

In particular, the resistive pressure represents the pressure difference required to generate a given gas flow rate within the airways, whereas the elastic pressure is the pressure needed to expand the lungs and chest wall. Indeed, we can describe the forces acting during ventilation by the simplified equation of motion of the respiratory system (Eq. 2):

$$P_{aw}(t) = P_0 + R \cdot \dot{V}(t) + \frac{V(t)}{C_{RS}} \quad (2)$$

Where R is the resistance of the airways (and the endotracheal tube in case of invasive ventilation), V is the lungs volume, $\dot{V}$ is the airflow, C_{RS} is the compliance of the respiratory system.

During MV the airways pressure $P_{aw}(t)$, needed to provide a respiratory act, is given by the sum of the pressure developed by the respiratory muscles and the pressure developed by the ventilator:

$$P_{aw}(t) = P_{vent}(t) + P_{musc}(t) = P_0 + R \cdot \dot{V}(t) + \frac{V(t)}{C_{RS}} \quad (3)$$

Eq. (3) describes the synergistic impact of both the patient's muscular effort and the pressure delivered by the ventilator on the respiratory system. The type of MV is defined by the balance between these two pressures: controlled ventilation, assisted ventilation or non-assisted ventilation.

This study concentrated on non-assisted ventilation, specifically CPAP therapy, and involved solving the equation of motion for the respiratory system using a multidomain 0D model. The time-varying curve of respiratory muscle activity ($P_{musc}(t)$) was incorporated as an input in the model to simulate the patient's spontaneous breathing. Meanwhile, the ventilator pressure ($P_{vent}(t)$) functioned to sustain a constant and positive airway pressure, compensating for the pressure fluctuations generated by the patient's breathing.

2.2 Multidomain 0D model

A lumped circuit model of the ventilation circuit (Figure 2) was developed in Mathworks® Simulink using the SimScape library to replicate the pneumatic scheme shown in Figure 1. For the purposes of this study, only the air properties (e.g., specific gas constant, dynamic viscosity, specific enthalpy) were considered and defined in the model, as the discussion regarding oxygen supply falls outside the scope of this research. The blower was simulated by inputting the performance curves provided in the datasheet of a selected commercial blower. A pressure sensor was employed to monitor the pressure at point A (Figure 2) and to adjust the blower rotational speed to maintain the pressure around the therapeutic value. This control was obtained by implementing a proportional-integral-derivative controller (P = 1.8, I = 0.7, D = 0). Circuit passive elements (i.e., filters, check valves, soda lime, safety valve, air leakage) were simulated using localized load losses and their pneumatic resistive behavior was characterized through *in vitro* tests performed on the corresponding commercial components. In detail, the pressure drop (measured with AMS 6915, OEM) at the ends of each component was recorded for different imposed flows (measured with FM3200, Sensirion); the resulting pressure-flow curves were interpolated using the descriptive curve of the "Flow Resistance" block:

$$\Delta p = \frac{\xi \dot{m}^2}{2\rho S}$$

where Δp is the pressure drop from port A to port B, ξ is the loss factor, $\dot{m}$ is the imposed flow, ρ is the fluid density, and S is the flow area. The pressure drops obtained for each component are reported in Table 1.

Table 1. Pressure drops for a nominal flow rate of 20 L/min

	Δp (cmH_2O)
Antiviral filter	0.27
Check valve	0.39
Soda lime	0.30
Safety valve	0.09
Interface leakage	150

In order to replicate the inspiratory and expiratory pipes, a length of 2 meters, an internal diameter of 15mm, and a roughness of 0.01mm were considered, with consistency with commercially available ventilation pipes. An aggregate equivalent length of 1 m was introduced to consider the pipe bending, in accordance with the *in vitro* tests. The low deformability of the interface, typically associated with helmet interfaces, was disregarded. In fact, once the helmet is fully expanded by positive pressure, any volume changes are negligible, as air compressibility dominates over helmet deformability. The same reasoning applies to balloons used as reservoirs. The check valves and the safety valve were represented as ideal in the model, since their pneumatic resistance behavior was considered through the inclusion of a "Flow Resistance" block for each valve.

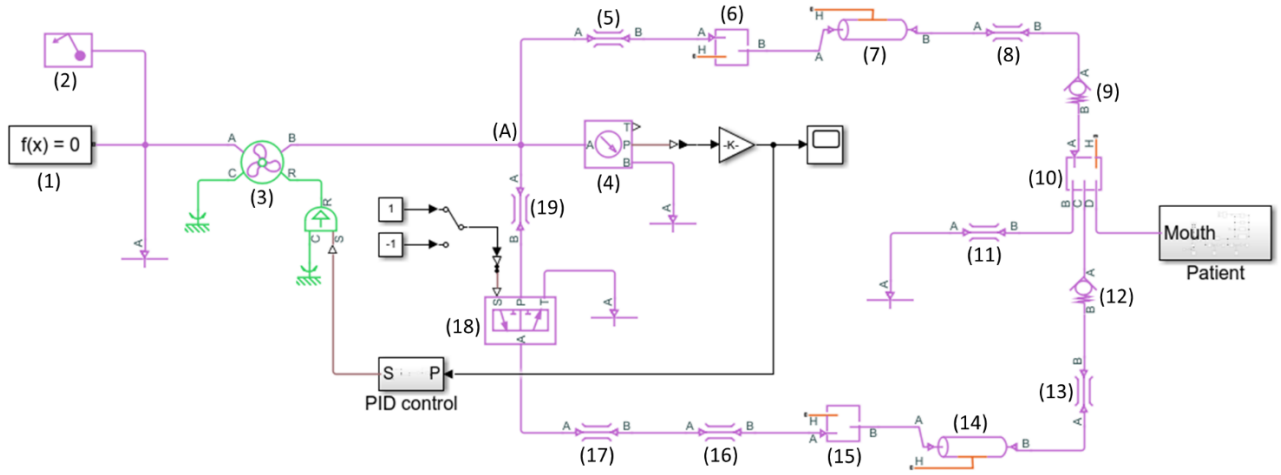

Figure 2. Graphics of the ventilation circuit model (SimScape): 1) Solver configuration, 2) gas property, 3) blower, 4) pressure and temperature sensor, 5) antiviral filter (insp.), 6) reservoir (insp.), 7) inspiratory pipe, 8) check valve resistance (insp.), 9) check valve (insp.), 10) patient interface, 11) leakage resistance, 12) check valve (exp.), 13) check valve resistance (exp.), 14) expiratory pipe, 15) reservoir (exp.), 16) soda lime, 17) antiviral filter (exp.), 18) safety valve, 19) safety valve resistance.

The model of the patient is reported in Figure 3. The extended RIC model was selected among the electric circuit-based linear 0D models of the respiratory system [27–30]. The airways were modelled as a localized load loss, and two sensors enabled the measurement of two key parameters: the pressure at the airway entrance (Paw) and the alveolar pressure (Palv), recorded at points A and B, respectively (Figure 3). The lungs were simulated as a plunger moving inside a cylinder. In parallel to this block, the model incorporates a spring, a damper and an actuator, to simulate the compliance of the lung-chest wall system, the damping of the lung tissue, and the effort exerted by the respiratory muscles, respectively. Whether in physiological resting conditions lung compliance can be adequately represented by a total respiratory compliance (Crs) exhibiting a linear behavior, in pathological conditions where CPAP therapy is administered a more complex non-linear description is required. Therefore, in this study the spring (block 23, Figure 3) has a non-linear mechanical behavior to replicate the characteristic sigmoid pressure-volume curve of the lung-chest wall system [31] (Figure 4). The curve was divided into three distinct segments, each approximated using a piecewise linear behavior. Three different compliances were assigned to these segments: a first compliance below the pressure at the lower inflection point (LIP) (Cl), a compliance between LIP and upper inflection points (UIP) (Cb), and a final compliance above UIP (Cu) [32]. This approach allowed for an accurate representation of the lung-chest wall system's behavior throughout the pressure-volume curve.

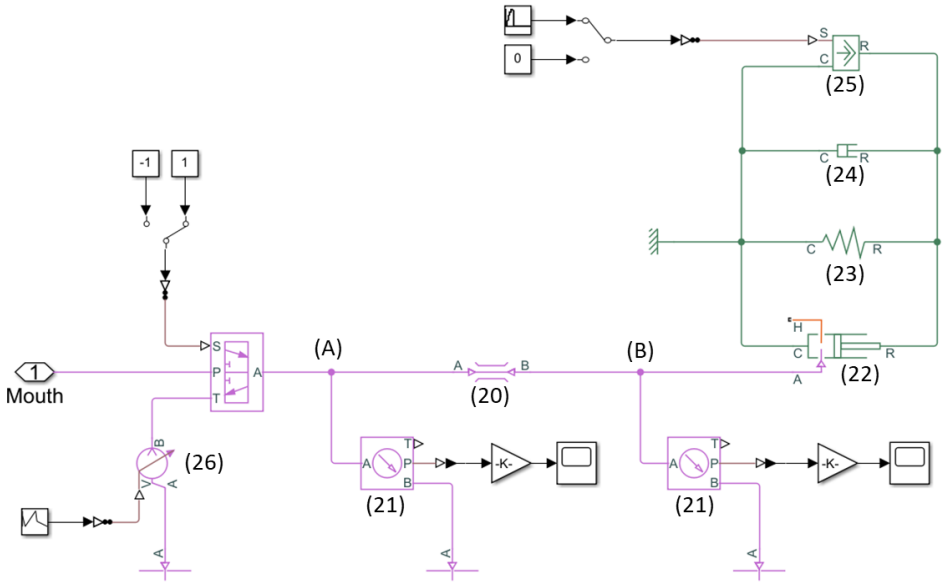

Figure 3. Graphics of the patient model (SimScape): 20) airways, 21) pressure and temperature sensor, 22) lungs, 23) lung compliance, 24) tissues damping, 25) respiratory muscles, 26) volume control insufflator.

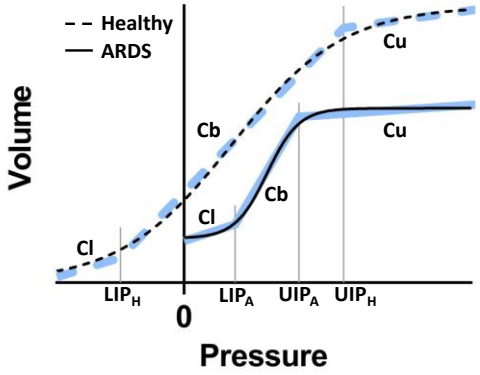

Figure 4. Pressure-Volume curves of the respiratory system. Sigmoidal curves in black [31], model approximation curves in blue. The subscript 'H' indicates a parameter related to the healthy subject, while the subscript 'A' indicates a parameter related to the ARDS subject. Negative pressures are never reached during spontaneous breathing at rest but only during a forced expiration.

The developed patient model permits to simulate not only a healthy condition but also pathological ones; in particular, the ARDS is characterized by a decrease of lung compliance and of the FRC and an increase of breath frequency. In addition, to test the reliability of the model in reproducing subjects with altered airway resistance, Chronic Obstructive Pulmonary Disease (COPD) was also considered in this work, although this condition is typically treated with NIV-CPAP only in cases of acute exacerbation. COPD is characterized by an increased flow resistance within the airways, that hinders complete expiration before the subsequent inhalation, resulting in hyperinflation and increased work of breathing due to an intrinsic PEEP (PEEPi). NIV can provide external PEEP to counterbalance PEEPi in patients with COPD and to offset the effects of an acute exacerbation in acidotic patients [12,33].

To populate patient specific lung parameters within the patient model, relations summarized in Table 2 were used, considering a predicted body weight (PBW) estimated according to the following simplified equations [34], where height is expressed in centimeters:

$$PBW\ in\ female\ (kg) = (height\ -\ 100) \cdot 0.9 - 5 \quad (4)$$

$$PBW\ in\ male\ (kg) = (height\ -\ 100) \cdot 0.9 \quad (5)$$

Specifically, the parameters refer to mild-to-moderate ARDS condition, which can be effectively treated with NIV-CPAP therapy in clinical practice [14–16]. Table 2 shows a 25% reduction in lung compliance in the ARDS patient compared to a healthy subject (Cl ARDS vs. Cb healthy) within the segment of the Pressure-Volume curves corresponding to positive pressures up to the patient's LIP (Figure 4), which includes the resting breathing condition. Beyond the LIP, the ARDS patient exhibits an approximately 35% increase in compliance relative to the healthy subject (Cb ARDS vs. Cb healthy), attributed to the progressive reopening of collapsed lung regions at positive pressures, primary goal of CPAP therapy.

Table 2. Lung parameters.

	Healthy	COPD	ARDS
Compliance between the LIP and the UIP, Cb (ml/mbar)	0.8·PBW [35,36]	0.9·PBW [36]	1.1·PBW [32]
Compliance below the LIP, Cl (ml/mbar)	*	*	0.6·PBW [36]
Compliance above the UIP, Cu (ml/mbar)	8 [37]	8 [37]	8 [37]
Lower Inflection Point, LIP (mbar)	*	*	8 [38]
Upper Inflection Point, UIP (mbar)	35 [37]	35 [37]	24 [37,38]
Tissues damping (mbar*s/L)	2 [24]	2 [24]	2 [24]
Airways resistance (mbar*s/L)	12 [35,36]	20 [36]	13 [36]
Functional Residual Capacity, FRC (ml)	27·PBW [35,39,40]	27·PBW [35,39,40]	17·PBW [39,41]

*The healthy and COPD subjects exhibit a LIP at negative pressures, so the parameters related to the LIP for these subjects was not considered in the model during spontaneous breathing at rest.

2.3 3-stages validation of the multidomain 0D model

After designing the multidomain 0D model, four distinct subjects were simulated: females with heights of 160cm and 170cm, males with heights of 175cm and 185cm. Each of these subjects, with their unique Crs and FRC values attributed in line with their specific heights, were modelled in the healthy and pathological conditions (Table 3). The respiratory rate was set to 12 breath per minute for healthy and COPD patients and 28 breath per minute for ARDS patients. The twelve cases constituted a dataset covering a wide range of lung parameters to test the model performance. In particular, the subjects present an increasing challenge (referring to Table 3) from left to right (increasing lung compliance and tidal volume) and from top to bottom (increasing complexity of lung mechanical behavior and respiratory frequency) regarding the control of CPAP therapy delivery by the device.

Table 3. Healthy and pathological subjects implemented. The table is organized based on the four subjects and the three conditions that were considered during the study.

	Female 160cm	Female 170cm	Male 175cm	Male 185cm
Healthy	C.1a	C.2a	C.3a	C.4a
COPD	C.1b	C.2b	C.3b	C.4b
ARDS	C.1c	C.2c	C.3c	C.4c

The closed-loop ventilation circuit [18] was then assembled *in vitro* using commercially available components and connected to a lung simulator able to replicate the twelve healthy and pathologic subjects (TestChest® V3, Organis Gmbh, CH). To ensure consistency and comparability, the same setup was employed for both *in vitro* tests and *in silico* simulations. This approach guarantees a reliable comparison between *in vitro* and *in silico* results across the twelve cases, enabling a 3-stages validation of the multidomain 0D.

The first stage focused on validating only the numerical passive behavior of the patient as if in a state of apnea. Experimentally, the lung insufflation was obtained with a 500 ml syringe moved at a constant speed. The measured inflow was given as input in the "Controlled Volumetric Flow Rate Source" block (block 26, Figure 3) as an external lung ventilation in the patient subroutine whose respiratory muscles were properly deactivated (block 25, Figure 3). Numerical and experimental data of both alveolar pressure and air volume inside the lung were compared generating a chart with the experimental results serving as the independent variable and the numerical results as the dependent variable; their similarity was assessed through a linear regression, comparing the data to the 45-degree line, which represents a perfect overlap ($R^2 = 1$).

The second stage was dedicated to the validation of the active patient during spontaneous breathing, which was generated by the activation of the respiratory muscles block. The effort of respiratory muscle was defined by an activation curve (Figure 5) [29], inserted in both the actuator block and in the lung simulator. The respiratory muscle pressure curve defines the phases of inspiration, expiration, and the pause in the respiratory cycle based on the patient's breathing rate, generating a flow through the airways with a more realistic non-sinusoidal profile. The flow passing through the patient's airway and the alveolar pressure were recorded and compared.

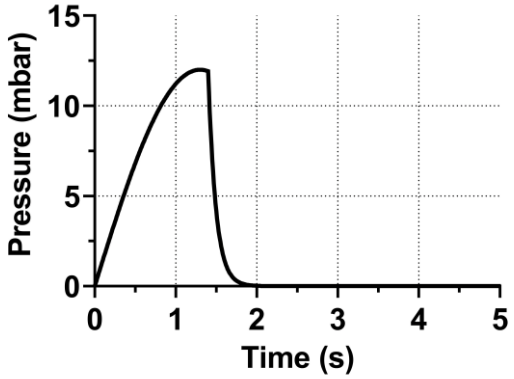

Figure 5. Muscles activation curve.

The third stage addressed the validation of the ensembled model with the patients spontaneously breathing in the ventilation circuit. Here, both the pressure sources were simultaneously activated (i.e., the patient's respiratory muscles and the external blower). The CPAP therapy level was set to 6 cmH_2O. The accuracy of the model in predicting the impact of ventilation on lungs was evaluated by comparing the alveolar pressure and the flow through the patients' airway.

2.4 NIV-CPAP ventilation circuit design

The validated multidomain 0D model was employed to guide the design of the ventilation circuit for the correct delivery of CPAP therapy to the patient, which was evaluated according to three key requirements. Specifically, the device: (1) must deliver the correct average positive pressure at the patient interface, (2) must maintain constant positive pressure throughout the respiratory cycle, and (3) must not restrict the patient’s breathing. These three design requirements were investigated by exploring the impact of three

correlated features, respectively: (1) the leakage amount at the patient interface, (2) the air volume within the circuit allowed by the interface dead volume and the presence of reservoirs, and (3) the amount of resistance induced by the circuit components.

2.4.1 Interface leakage

Leaks refer to the unintended escape of air from the interface, causing airflow through the inspiratory limb. This airflow leads to a pressure drop from the ventilator to the interface, which can reduce the static pressure within the interface and consequently impact the delivery of the therapy to the patient. Interface leakage was modelled by varying the patient interface resistance (block 11, Figure 2). The resulting decrease of static pressures was quantified at three different therapeutic CPAP levels (5, 10 and 15 cmH_2O) under three different interface leakage conditions: low leak (150 cmH_2O, as detailed in Table 1 for the patient interface resistance, resulting to 5, 8 and 9 L/min of leak for 5, 10 and 15 cmH_2O of CPAP, respectively), moderate leak (30 cmH_2O, resulting to 12, 17 and 21 L/min of leak), marked leak (15 cmH_2O, resulting to 17, 23 and 29 L/min of leak). In this section, the respiratory muscles were deactivated (block 25, Figure 3) because assessing static pressure does not involve the patient's breathing.

2.4.2 Interface dead volume and reservoirs

Patient interfaces with a larger volume, such as the helmet interface, enable the attenuation of pressure fluctuations caused by the patient's breathing. This, in turn, helps maintain a more constant positive pressure in the airways throughout the entire breathing cycle. In this analysis, pressure oscillations were investigated at 5, 10 and 15 cmH_2O of CPAP level, using a total face mask and a helmet interface. The interface was modelled by varying the volume in the patient interface (block 10, Figure 2). Additionally, we evaluated the effect of including a 6 L volume reservoir in both limbs of the ventilation circuit (blocks 6 and 15, Figure 2). The most critical patient (C.4c characterized by the highest respiratory rate and tidal volume) was selected to conduct the analysis. Taking into account the patient's gradual adaptation to CPAP therapy and the subsequent improvement of his pathological condition, the patient was also evaluated at a reduced respiratory rate (20 breaths/min) (defined as C.4d). This case permitted to assess the effect of different respiratory rates on oscillation attenuation.

2.4.3 Ventilation circuit resistance

During ventilation, the patient needs to overcome the additional resistances introduced by the ventilation circuit to breathe effectively. When this doesn't occur, patients may be unable to complete the breathing cycle, resulting in air retention in the lungs. This condition causes a reduction in tidal volume and the generation of PEEPi and is more common in patients with a high respiratory rate [42]. These two parameters were used to quantify the negative impact of the ventilation circuit on the patient's breathing. Specifically, to explore tidal volume reduction, the turbine (block 3, Figure 2) was deactivated. This allowed the evaluation of patient's lung volume without the beneficial effect of CPAP therapy, which helps recruiting collapsed alveoli. Hence, different ventilation circuits were created to quantify the impact of their configuration (in terms of number of components and their arrangements) on patients' tidal volume and end-expiratory alveolar pressure during NIV-CPAP treatment. Table 4 summarizes the studied circuit configurations.

Table 4: Ventilation circuit configurations analyzed within the multidomain 0D model.

ID*	Description
CC	Patient spontaneously breathing without the ventilation circuit (Control Case)
VC	The starting ventilation circuit, as described in section 2.2
VCti	The length of the pipe in the inspiratory limb has been doubled to allow for device placement on one side of the patient.

VCte	The length of the pipe in the expiratory limb has been doubled to allow for device placement on one side of the patient.
VCtei	The length of the pipe in both limbs has been doubled to allow for device placement on both sides of the patient.
VCfi	An additional antiviral filter has been inserted into the inspiratory limb to enhance viral isolation of the device.
VCfe	An additional antiviral filter has been inserted into the expiratory limb to enhance viral isolation of the device.
VCfei	Additional antiviral filters have been inserted in both limbs to enhance viral isolation of the device.
VCteifei	The length of the pipe in both limbs has been doubled to allow for device placement on both sides of the patient, and additional antiviral filters have been inserted in both limbs to enhance viral isolation of the device.
VCtife	The balanced ventilation circuit, characterized by a doubled length of the pipe in the inspiratory limb and an additional antiviral filter in the expiratory limb.

* CC: Control Case; VC: Ventilation Circuit; t: doubled tubing length; f: doubled filters; i: inspiratory limb; e: expiratory limb

3 Results

The 3-stages validation of the multidomain 0D model resulted in optimal consistency with *in vitro* tests. Regarding the validation of the passive behavior of the patient (Figure 6a), the correlation coefficient R^2 values are nearly 1 for all the twelve cases, indicating a high degree of overlap between *in silico* and *in vitro* results. The second stage addressed the model validation in spontaneous breathing, which suggests strong reliability with R^2 coefficient values exceeding 0.93 for the alveolar pressures and 0.94 for the flows passing through the patient's airway (Figure 6b). Connecting the spontaneously breathing patient to the ventilation circuit (Figure 6c) remarkable good performances in computing flows (R^2 = 0.90), and pressure (R^2 = 0.97) were obtained.

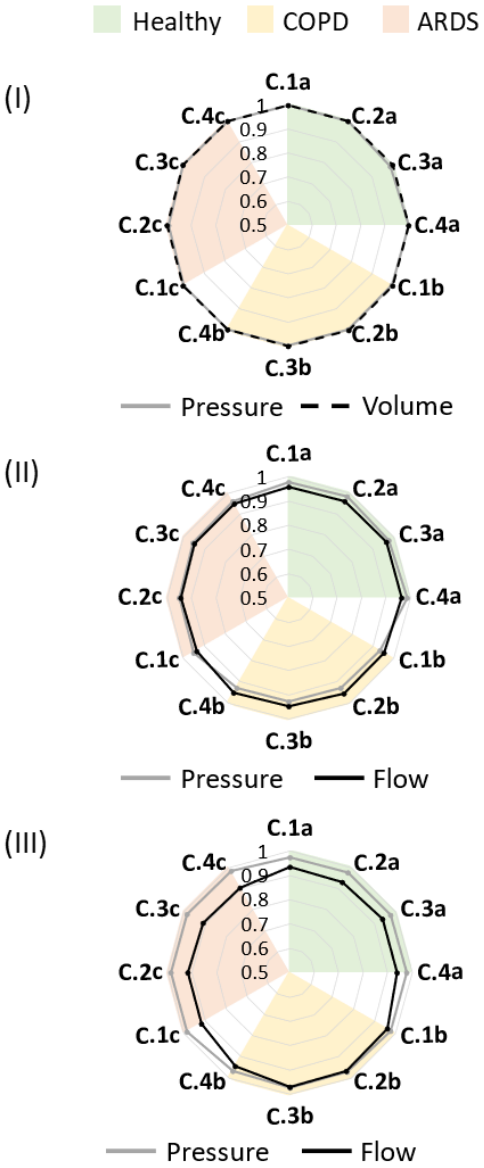

Figure 6. R^2 results for the 3-stages validation of the multidomain 0D model. (I) stage: Validation of the patients' passive behavior; (II) stage: Validation of the active patient during spontaneous breathing; (III) stage: Validation of the active patient breathing in the ventilation circuit. Detailed results are described in the Supplementary Materials.

Table 5 lists the static pressures calculated at the interface varying the extent of leakage at the patient interface. It can be observed that a greater degree of leakage results in a more substantial reduction of the positive pressure at the interface: approximately 1%, 3%, and 6%, for low, moderate, and marked leak respectively. In terms of percentages, there is no apparent correlation between the pressure decrease and the set pressure value. However, in absolute terms, the most significant reduction, approximately 1 cmH_2O, occurs when the CPAP level is set at 15 cmH_2O and there is marked leak at the interface.

Table 5. Static pressures calculated at the interface (cmH_2O) under varying interface leakage conditions.

	Low leak	Moderate leak	Marked leak
5 cmH_2O	4.96	4.83	4.68
10 cmH_2O	9.92	9.67	9.38
15 cmH_2O	14.89	14.52	14.07

Concerning the effect of the air volume accommodated within the circuit, Figure 7 shows that the use of the helmet interface reduces pressure oscillations by approximately 8% with respect to the total-face mask in both cases C.4c and C.4d. Furthermore, the addition of reservoirs to the limbs of the ventilation circuit allows a reduction of the oscillations by about 3% with the mask and approximately 6% with the helmet for C.4c, and about 1% with both interfaces for C.4d. Also, these outcomes don't exhibit a dependency on the set CPAP level. Moreover, Figure 7 confirms the influence of the breathing rate on pressure oscillations: the higher the patient's breathing rate, the more the oscillations are attenuated.

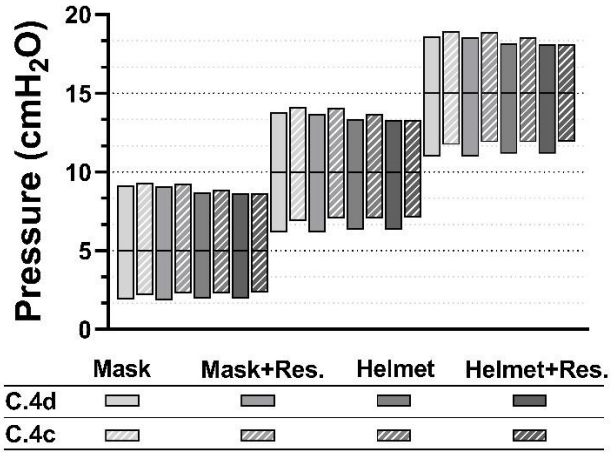

Figure 7. Pressure fluctuations in the presence of different interface volumes (i.e., mask or helmet) and with or without the addition of reservoirs. The results represent the range between the minimum and maximum pressures reached during patient breathing at both 28 breaths/min (C.4c, patterned filled bars) and at 20 breaths/min (C.4d, uniform filled bars).

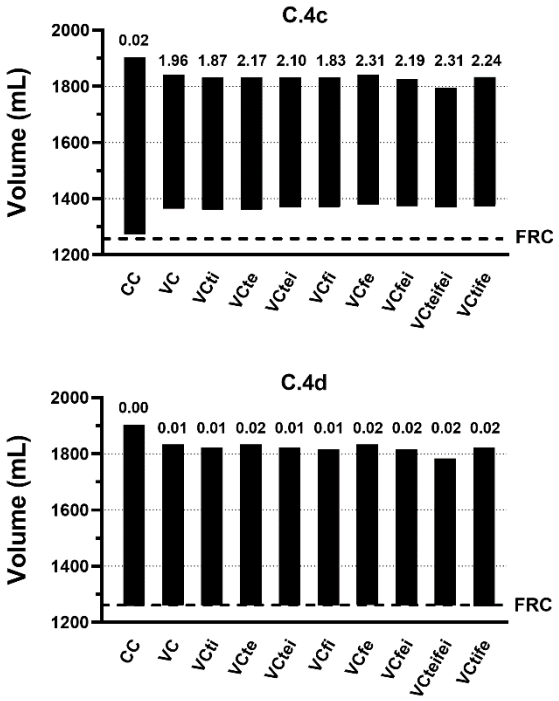

Figure 8. Range between the minimum and maximum volume reached during patient breathing at both 28 breaths/min (C.4c, top bar plot) and at 20 breaths/min (C.4d, bottom bar plot) and PEEPi (numeric values above bars, cmH_2O) for the nine ventilation circuit configurations analyzed within the multidomain 0D model.

Finally, Figure 8 illustrates the resistive effect of the circuit configurations on the patient's breathing. When connected to the therapy device, indeed, the respiratory muscles must overcome both airway and ventilation circuit resistances. In all the configurations proposed, a significant reduction in tidal volume (bar length) can be observed, averaging around 15% for case C.4c and around 28% for case C.4d. The decrease in tidal volume can be attributed to two aspects: the reduction of the lung volume at the end of the inspiratory phase (maximum bars value in figure) and the increase of the lung volume at the end of the expiratory phase (minimum bars value in figure). The first one can be primarily attributed to the delayed entry of air into the alveoli due to increased resistances met by the patient's inspiration. Consequently, the expiratory phase begins before the inspiratory phase has completed alveolar filling. The second one is related to a certain amount of air being trapped inside the lung at the end of the expiratory phase, maintaining positive alveolar pressure (PEEPi). In case C.4d, this second aspect is negligible, with associated PEEPi values ranging from 0.01 to 0.02 cmH_2O. Conversely, in case C.4c, the patient already exhibited a minimal PEEPi of 0.02 cmH_2O during spontaneous breathing, and the connection to the ventilation circuit produces a substantial PEEPi of approximately 2 cmH_2O, which varies based on the specific configuration under consideration. As a result of heightened resistance encountered during the patient's exhalation, the high respiratory rate of this patient triggers the initiation of the inspiratory phase before the expiratory phase is fully completed.

Additionally, comparing the circuit configurations, an increase in PEEPi can be observed in configurations with greater resistance in the expiratory limb (VCte, VCtei, VCfe, VCfei), while the circuit configuration has a minimal influence on the reduction of tidal volume, with a maximum variation of 23 ml. In particular, a lower PEEPi value is observed in configurations with higher resistance in both limbs (VCtei, VCfei) compared to configurations with higher resistance only in the expiratory limb (VCte, VCfe), despite having more overall resistances in the circuit. On the other hand, the VCtetfei configuration stands out as an exception, showing a more significant reduction in tidal volume, approximately 40 ml for both patients, and a PEEPi of 2.31 cmH_2O for case C.4c, due to a more pronounced increase in resistances within the circuit. These

findings highlight the advantage of balancing the resistances between the limbs but increasing the resistances in the circuit only where necessary.

4. Discussion

In the present study, a multidomain 0D model capable of predicting the pneumatic behavior of a closed-loop NIV-CPAP ventilation device was developed and validated through experimentally obtained data. In order to validate the model, the simulation results, in terms of pressures, volumes, and flows, were compared with in vitro tests conducted using a lung simulator, and optimal agreement was achieved between the in silico prediction and simulator outputs, quantified through curve similarity (R^2).

A 0D in silico model has been employed in numerous studies to investigate the impact of MV on simulated patients [20–26]. In four publications [20–23] various ventilation modes were simulated and their control algorithms were investigated; however, only the pressure exerted by the ventilator on the patient was replicated. In other three publications [24–26], instead, the pneumatic circuit of the ventilator was also considered, focusing on IMV provided in pressure-controlled continuous mandatory ventilation or volume-controlled continuous mandatory ventilation modes. In this work, a ventilation system for NIV-CPAP applied to spontaneously breathing patients was considered. In order to accurately simulate patients treated in NIV-CPAP mode, a novel sigmoidal model of lung compliance and a non-sinusoidal respiratory muscle pressure curve were employed. Results showed that this strategy permitted the successful description of patients with different lung compliances and airway resistances spanning various respiratory conditions that can be treated with CPAP therapy. To the best of the authors' knowledge, there are currently no tools available in literature that facilitate the investigation and optimization of non-invasive ventilation systems. Indeed, this study introduces the first mathematical model designed to simulate the performance of a ventilation system with a spontaneously breathing patient.

Regarding the study of the identified design requirements of the device, the impact of interface leakage on the delivered therapeutic static pressure resulted in acceptable reductions, even under conditions of marked leak (approximately 6% reduction), with air leaks of almost 30 L/min [43]. Therefore, this result supports the possibility of adopting interfaces that typically show significant leaks (e.g., oro-nasal or full-face masks) with the device. Any potential increase in leakage effects observed in future clinical experiments could possibly be mitigated by relocating the pressure sensor used in the turbine control algorithm to the patient interface. This adjustment would allow the turbine to directly regulate the pressure at the interface, effectively compensating for leakage effects. The increase in air volume within the circuit, analyzed by changing the interface (replacing the mask with a helmet) and adding reservoirs to the inspiratory and expiratory limbs, resulted in a higher reduction in pressure oscillations with the increase of the patient breathing rate. This phenomenon can be explained by the capacitive behavior of the air that accumulates within the interface and the reservoirs. Indeed, the air compressibility attenuates the pressure oscillations, acting as a low-pass filter with respect to pressure. However, the reduction was evaluated as negligible, and therefore it was decided to remove the reservoirs, which had the added benefit of reducing the size of the ventilation circuit with positive implications for the patient's comfort and usability.

The investigation of the impact of circuit components resistance on the patient's spontaneous breathing revealed that the mere introduction of a ventilation circuit induced the generation of PEEPi, which increased with higher respiratory rate. It's crucial to highlight that the results and observations are intricately tied to the respiratory muscle pressure curve (Figure 5), pointing out the importance of adopting a more realistic non-sinusoidal profile. During NIV-CPAP therapy, inspiratory effort plays a crucial role in investigating the risk of self-inflicted lung injury [44,45]. Specifically, in Menga et al. [44], pressure swings were analyzed in fifteen hypoxemic patients treated with CPAP, yielding an average esophageal pressure variation of 13 cmH_2O and a transpulmonary pressure variation of 12 cmH_2O. These results align with the

peak of the muscular effort curve reported in Figure 5 (12 mbar, approximately 12.24 cmH_2O). Increasing resistances in the inspiratory and expiratory limbs resulted in minimal additional impairments in the simulated patient's lung ventilation. However, the generation of a lower PEEPi was observed when balancing the resistances between the limbs, leading to the selection of an optimized configuration (VCtife). This configuration included doubling the length of the tubes in the inspiratory limb to allow for device placement beside the patient and easy interface connection, as well as adding a second antiviral filter in the expiratory limb to enhance viral isolation of the device from the patient's expired gases.

The use of a 0D model for the respiratory system, which lacks the description of the bronchial tree's geometry, does not allow for the investigation of localized effects of ventilation in various lung segments. In the literature, several 3D models are available that take into account lung geometry obtained from CT-scan imaging [46–51]. However, the use of lumped elements ensures high computational-cost efficacy, with at most 2 seconds per simulated second of breathing. As an additional limitation of the model, the deformability of the reservoir walls was not simulated. Introducing reservoir compliance would complicate the model and significantly increase computation times, negating the advantages of using the lumped parameters described above. Furthermore, the model provides an analysis from a pneumatic perspective and does not simulate metabolism or gas exchange in the alveoli, thus not accounting for the therapeutic effect of oxygen supply. Future developments will focus on studying oxygen supply and blood oxygenation through the creation of a cardiopulmonary model of the patient [52–56]. The study conducted in this work presents some limitations. Firstly, it is confined to a limited number of patients and is restricted to an adult population. The range of tidal volumes, compliance, inspiratory effort and pressure swings analyzed does not encompass the full spectrum of clinical conditions typically encountered in intensive care units (e.g., neonatal application [57–60]). Secondly, the study focuses solely on evaluating the performance of the ventilation circuit proposed in [18], without comparing it to other devices commonly used in clinical practice for CPAP therapy delivery [61]. Despite these limitations, the use of lumped elements offers the flexibility in easily modifying circuit components, making it possible to adapt the model to various non-invasive ventilation systems and patient parameters. This adaptability broadens the model's applicability to a wider range of patients. Consequently, the proposed multidomain 0D model demonstrates strong reliability for future applications, providing valuable insights on the delivery of the ventilation therapy and the impact of circuit components on device performance.

5. Conclusion

The multidomain 0D model developed in this study demonstrated its capability to accurately replicate different patients during spontaneous breathing. In addition, this tool solved the equation of motion of the respiratory system, analyzing the synergistic impact of both the patient's muscular effort and the positive pressure delivered by a NIV system on the lung. This analysis allowed to investigate the impact of circuit components arrangements on the efficacy of CPAP administration (i.e., interface leakage, air volume within the circuit, components resistance) using a novel closed ventilation circuit. Moreover, the strong agreement between the *in silico* and *in vitro* data, indicated the accuracy and reliability of adopting the multidomain 0D modelling approach. In conclusion, this model demonstrated its effectiveness as a valuable tool for guiding the design of an innovative device, and the optimization of non-invasive ventilation circuits, with high computational efficiency, flexibility, and reliability.

Data availability

The majority of the data generated and analyzed during this study is included in the published article and its supplementary file. Any additional data is available from the corresponding author upon reasonable request.

Acknowledgements

This publication is part of the project NODES which has received funding from the MUR – M4C2 1.5 of PNRR funded by the European Union - NextGenerationEU (Grant agreement no. ECS00000036). The author MDL is supported under Ministerial Decree No. 1061/2021 within the framework of the FSE REACT-EU program - PON Research and Innovation 2014-2020. The author GP is supported under Ministerial Decree No. 1062/2021 within the framework of the FSE REACT-EU program - PON Research and Innovation 2014-2020. The author RV is (partially) supported by the Italian Ministry of University and Research (MUR) program "Departments of Excellence 2023–2027", AGING Project – Department of Translational Medicine, Università del Piemonte Orientale.

Declaration of interests

All Authors except CO and RV declare that they have no known competing financial interests or personal relationships that could have appeared to influence the work reported in this paper. CO participated to the development of an interface for NIV, and receives royalties from Intersurgical SpA for that invention. RV received honorarium for lecture from Intersurgical (2021).

Author contributions

AF: Conceptualization, Methodology, Writing - Original Draft. MDL: Validation, Investigation. SB: Visualization, Writing - Original Draft. GP: Conceptualization, Formal analysis. NDV: Investigation, Writing - Review & Editing, FM: Investigation, Writing - Review & Editing, FDC: Resources, Writing - Review & Editing, RV: Resources, Writing - Review & Editing. ALA: Project administration, Funding acquisition. CO: Conceptualization, Writing - review & editing. MT: Supervision, Visualization, Writing - review & editing.

References

[1] T. Pham, L.J. Brochard, A.S. Slutsky, Mechanical Ventilation: State of the Art, Mayo Clin. Proc. 92 (2017) 1382–1400. https://doi.org/10.1016/j.mayocp.2017.05.004.

[2] T.C. Hardcastle, D.J.J. Muckart, R.V. Maier, Ventilation in Trauma Patients: The First 24 h is Different!, World J. Surg. 41 (2017) 1153–1158. https://doi.org/10.1007/s00268-016-3530-1.

[3] K. Asehnoune, P. Rooze, C. Robba, M. Bouras, L. Mascia, R. Cinotti, P. Pelosi, A. Roquilly, Mechanical ventilation in patients with acute brain injury: a systematic review with meta-analysis, Crit. Care 27 (2023) 221. https://doi.org/10.1186/s13054-023-04509-3.

[4] N. Farzan, S. Vahabi, S.S. Hashemi Madani, B. Farzan, Evaluating characteristics associated with the mortality among invasive ventilation COIVD -19 patients, Ann. Med. Surg. 69 (2021). https://doi.org/10.1016/j.amsu.2021.102832.

[5] A. Zhou, Q. Song, Y. Peng, D. Deng, X. Liao, P. Huang, W. Liu, Z. Xiang, Q. Liu, M. Jiang, X. Huang, X. Xiang, H. Peng, P. Chen, The Effect of Noninvasive Ventilation Support on COVID-19 Patients and Risk Factors for Invasive Ventilation – A Retrospective and Multicenter Study, Int. J. Gen. Med. Volume 14 (2021) 6085–6092. https://doi.org/10.2147/IJGM.S327429.

[6] M.C. Chang, T.U. Kim, D. Park, National early warning score on admission as risk factor for invasive mechanical ventilation in COVID-19 patients: A STROBE-compliant study, Medicine (Baltimore) 100 (2021) e25917. https://doi.org/10.1097/MD.0000000000025917.

[7] M.C. Chang, Y.-K. Park, B.-O. Kim, D. Park, Risk factors for disease progression in COVID-19 patients, BMC Infect. Dis. 20 (2020) 445. https://doi.org/10.1186/s12879-020-05144-x.

[8] J.A. Garcia-Gordillo, A. Camiro-Zúñiga, M. Aguilar-Soto, D. Cuenca, A. Cadena-Fernández, L.S. Khouri, J.N. Rayek, M. Mercado, The ARMII Study Group, COVID-IRS: A novel predictive score for risk of invasive mechanical ventilation in patients with COVID-19, PLOS ONE 16 (2021) e0248357. https://doi.org/10.1371/journal.pone.0248357.

[9] A.G.B. Broadhurst, C. Botha, G. Calligaro, C. Lee, U. Lalla, C.F.N. Koegelenberg, P.D. Gopalan, I.A. Joubert, G.A. Richards, B.W. Allwood, The optimal management of the patient with COVID-19 pneumonia: HFNC, NIV/CPAP or mechanical ventilation?, Afr. J. Thorac. Crit. Care Med. (2022) 119–128. https://doi.org/10.7196/AJTCCM.2022.v28i3.241.

[10] L. Brochard, A. Slutsky, A. Pesenti, Mechanical Ventilation to Minimize Progression of Lung Injury in Acute Respiratory Failure, Am. J. Respir. Crit. Care Med. 195 (2017) 438–442. https://doi.org/10.1164/rccm.201605-1081cp.

[11] International Consensus Conferences in Intensive Care Medicine: Noninvasive Positive Pressure Ventilation in Acute Respiratory Failure, 163 (2001).

[12] P. Popowicz, K. Leonard, Noninvasive Ventilation and Oxygenation Strategies, Surg. Clin. North Am. 102 (2022) 149–157. https://doi.org/10.1016/j.suc.2021.09.012.

[13] Z. Wang, Y. Wang, Z. Yang, H. Wu, J. Liang, H. Liang, H. Lin, R. Chen, Y. Ou, F. Wang, Y. Wang, Y. Wang, W. Luo, N. Li, Z. Li, J. Xie, M. Jiang, S. Li, The use of non-invasive ventilation in COVID-19: A systematic review, Int. J. Infect. Dis. 106 (2021) 254–261. https://doi.org/10.1016/j.ijid.2021.03.078.

[14] D.L. Grieco, S.M. Maggiore, O. Roca, E. Spinelli, B.K. Patel, A.W. Thille, C.S.V. Barbas, M.G. De Acilu, S.L. Cutuli, F. Bongiovanni, M. Amato, J.-P. Frat, T. Mauri, J.P. Kress, J. Mancebo, M. Antonelli, Non-invasive ventilatory support and high-flow nasal oxygen as first-line treatment of acute hypoxemic respiratory failure and ARDS, Intensive Care Med. 47 (2021) 851–866. https://doi.org/10.1007/s00134-021-06459-2.

[15] A. Pagano, G. Porta, G. Bosso, E. Allegorico, C. Serra, F. Dello Vicario, V. Minerva, T. Russo, C. Altruda, P. Arbo, V. Mercurio, F.G. Numis, Non-invasive CPAP in mild and moderate ARDS secondary to SARS-CoV-2, Respir. Physiol. Neurobiol. 280 (2020) 103489. https://doi.org/10.1016/j.resp.2020.103489.

[16] G.D. Perkins, C. Ji, B.A. Connolly, K. Couper, R. Lall, J.K. Baillie, J.M. Bradley, P. Dark, C. Dave, A. De Soyza, A.V. Dennis, A. Devrell, S. Fairbairn, H. Ghani, E.A. Gorman, C.A. Green, N. Hart, S.W. Hee, Z. Kimbley, S. Madathil, N. McGowan, B. Messer, J. Naisbitt, C. Norman, D. Parekh, E.M. Parkin, J. Patel, S.E. Regan, C. Ross, A.J. Rostron, M. Saim, A.K. Simonds, E. Skilton, N. Stallard, M. Steiner, R. Vancheeswaran, J. Yeung, D.F. McAuley, RECOVERY-RS Collaborators, N. Duffy, M. Kelly, D. Concannon, K. Ferguson, D. McClintock, R. Jha, V. Krishnamurthy, S. O'Farrell, C. O'Kane, C. Ross, R.D. Turner, S. Miodragovic, P. Hawkins, J. Welbourne, C. Wells, L. Lankester, S.D. Waddy, J. Lentaigne, J. Nesbitt, S. Clarke, C. Houghton, D. O'Riordan, K. Shepherd, B. Turnpenny, R. Joseph, M. Steiner, C. Rossall, R. Mundin, S. Boschi, H.J.C. McAuley, R.J. Russell, S. Diver, O. Elneima, W. Ibrahim, A. Yousuf, S. Edwards, M. Saim, B. Hopkins, L. Kelly, D. Lenton, H. Shackleford, L. Thrasyvoulou, H. Willis, S. Fairbairn, C. Green, M. Patel, L. Linhartova, E. Hayton, A. Chue, B. Collins, M. Page, E. Birkhamshaw, M. Bellamy, H. Bancroft, E. Gallagher, P. Antoine-Pitterson, B. Jones, S. Begum, S. Dhani, M. Crooks, K. Brindle, S. Faruqi, R. Flockton, E. Pinder, S. Thackray-Nocera, K. Dalemo, J. Doidge, J. Edwards, J. Douse, S. Bell, B. Purewal, C. Chabo, C. Buckman, D. Beeby, G. Gray, R. Francis, V. Rivers, M. Burton, N. Innes, S. Ghattas, R. Rabbani, V. Mahadevan, V. Mahadevan, A. Green, B. Burton, C. Hacon, E. Wilhelmsen, P.R. Hughes, K. Lee, R. Lowsby, L. Baker, P. Board, V. Chauhan, S. Clarke, D. Fullerton, C. Gabriel, T. Houston, D. Lees, R. Normanton, K. Pagett, S. Thornley, H. Wright, A. McMillan, M. Babores, X. Lee, T. Nagarajan, M. Holland, T. Sanctuary, R. Innes, S. Fletcher, N. Sehgal, T. Duncan, J. Pooley, E. Watkins,

H. Moudgil, M. Carnahan, D. Donaldson, D. Rao, C.L. Tey, L. Linkson, T. Buttle, J. Vidler, N. Griffiths, A. Hicks, H. Rupani, A. Alfridi, D. Barns, E. Cowan, M. David, A. Darbyshire, B. Giles, C. Roberts, C. Lameirinhas, D. Neville, E. Hossain, F. Thompson, H. Edwards, J. Naftel, J. Winter, K. Burrows, L. Wiffen, L. Fox, L. Murray, L. Hawes, M. Mamman, M. Moon, M. White, M. Rowley, N. Szarazova, S. Gosling, S. Cooper, S. Baryschpolec, S. Arndtz, Y. H-Davies, Y.A. El Khaleq, Z. Garner, S. Vythilingam, Y. Yang, D. Parekh, S. Madathil, J. Patel, C. Bergin, M. Bates, C. McGhee, D. Lynch, K. Bhandal, K. Tsakiridou, A. Bamford, L. Cooper, T. Whitehouse, T. Veenith, E. Forster, S. Lane, N. Adams, S. MacDonald, S. Manan, S. Lugg, P.A. Shah, E. McKemey, L. Crowley, G. Mussawar, A. Gogokhia, S. Gompertz, C. Snelson, T. Oelofse, J. Wilson, M. Bangash, S.S. Huq, F. Rauf, D. Dosanjh, N. Salmon, J. Tengende, K.F. Senior, B. Cooper, B. Sutton, I. Woolhouse, A. Crawshaw, R. Thompson, P. Glynn, J. Naylor, J. Alderman, M. Chotalia, M. Le Breuilly, N. Talbot, G. Packer, C. Carlin, D. Harvey, A. Gray, M. Gautam, I. Welters, D.O. Hamilton, H. Burhan, K. Hunter, B. Johnston, M. Lopez, C. Lowe, S. Mulla, J.F. Roman, D. Shaw, A. Waite, V. Waugh, K. Williams, A.K. Simonds, K.C. Tatham, E. Black, S. Jhanji, G. Ng Man Kwong, B. Messer, A. De-Soyza, P. McAlinden, S.D. West, V. Anumakonda, P. Dark, L. McMorrow, T. Marsden, N. Proudfoot, B. Charles, J. Pendlebury, B. Blackledge, A. Harvey, K. Knowles, R. Doonan, S. Lee, J. Perez, M. Slaughter, M. Taylor, V. Thomas, E. Hardy, N. Bakerly, L. Catlow, N. Majeed, D. Horner, L. Ali, D. Hutchinson, L. Fuller, J. Dodd, R. Bhatnagar, A. Clive, H. Adamali, A. Bibby, D. Higbee, H. Welch, E. Gendall, L. Staddon, A. Morley, S. Clarke, K. Smith, E. Perry, N. Rippon, L. Jennings, L. Solomon, K. Alloway, H. Lee, V. Sandrey, K. Bradburn, A. Milne, E. Goff, R. Williams, M. Ahmed, S. Bloch, A. Zaki, A. Roy, A. Rostron, L. Woods, F. Wakinshaw, P. Bainbridge, P. Hersey, M. Carpenter, C. Leech, L. O'Connor, A. Morrison, E. Rodgers, P. McAndrew, G. Lear, J. Coates, M. Richardson, D. Smith, W. Green, S. Murray, C. Pennington, H. De Wong, D. Land, H. Wheeler, M. Harvey, M. Watson, M. Brown, B. Irving, J. Bigg, M. Felongco, J. Mackenzie, D. Dhasmana, R. Thompson, P. Lui, F. Adam, F. Davey, J. Penman, A. McGregor, P. Cochrane, K. Shalan, W. Bozic, J. Brown, J. Carey, C. Daffern, E. Dight, M. Gane, B. Ghuman, J. Grummett, J. Guck, L. Hamilton, C. Hill, M. Hill, C. Muthiah, E. Padfield, J. Rai, K. Raynes, G. Scott, E. Stimpson, N. Strickland, A. Willis, J. Wood, B. Attwood, I. Atwal, P. Parsons, R. Vancheeswaran, S. Konda, Y.M.M. Myint, M. Mehta, A. Muhammad, A. Navarro, A. Rochester, S. Sundayi, M. Patel, A. Smith, C. Stewart, M. Tate, E. McGarry, C. (Rebecca) Pearson, B. Walsh, L. Glass, K. Black, S. Clements, R. Boyle, C. MacDonald, L. Hamilton, G. Moreland, R. Hamill, H. Reddy, S. Smuts, A. Bentley, Effect of Noninvasive Respiratory Strategies on Intubation or Mortality Among Patients With Acute Hypoxemic Respiratory Failure and COVID-19: The RECOVERY-RS Randomized Clinical Trial, JAMA 327 (2022) 546. https://doi.org/10.1001/jama.2022.0028.

[17] G. Bellani, S. Isgrò, R. Fumagalli, Helmet Continuous Positive Airway Pressure: Theory and Technology, in: A.M. Esquinas (Ed.), Noninvasive Mech. Vent., Springer Berlin Heidelberg, Berlin, Heidelberg, 2010: pp. 7–12. https://doi.org/10.1007/978-3-642-11365-9_2.

[18] M. Cavaglià, C. Olivieri, U. Morbiducci, T. Raparelli, G. Jacazio, A. Ivanov, A. Chiesa, D. Savino, S.M. Chiarenza, A. Romiti, A. Romiti, M. Ferrara, G. Musso, A. Audenino, Noninvasive mechanical ventilation in the COVID-19 era: Proposal for a continuous positive airway pressure closed-loop circuit minimizing air contamination, oxygen consumption, and noise, Artif. Organs 45 (2021) 754–761. https://doi.org/10.1111/aor.13888.

[19] A. Audenino, T. Raparelli, U. Morbiducci, M. Cavaglià, A. Ivanov, A. Romiti, A. Romiti, M. Ferrara, A. Chiesa, CPAP kit to support breathing, Patent cooperation treaty (2022), WO2022079642A1.

[20] N.Q. Al-Naggar, H.Y. Al-Hetari, F.M. Al-Akwaa, Simulation of Mathematical Model for Lung and Mechanical Ventilation, J. Sci. Technol. 21 (2016) 1–9. https://doi.org/10.20428/jst.v21i1.1017.

[21] E. Dincel, Advanced mechanical ventilation modes: design and computer simulations, Comput. Methods Biomech. Biomed. Engin. 24 (2021) 673–686. https://doi.org/10.1080/10255842.2020.1845319.

[22] L.Y. Serna, A.M. Hernandez, M.A. Mañanas, Computational tool for modeling and simulation of mechanically ventilated patients, in: 2010 Annu. Int. Conf. IEEE Eng. Med. Biol., IEEE, Buenos Aires, 2010: pp. 569–572. https://doi.org/10.1109/IEMBS.2010.5626429.

[23] A.S. Tran, H.Q. Thinh Ngo, V.K. Dong, A.H. Vo, Design, Control, Modeling, and Simulation of Mechanical Ventilator for Respiratory Support, Math. Probl. Eng. 2021 (2021) 1–15. https://doi.org/10.1155/2021/2499804.

[24] J. Giri, N. Kshirsagar, A. Wanjari, Design and simulation of AI-based low-cost mechanical ventilator: An approach, Mater. Today Proc. 47 (2021) 5886–5891. https://doi.org/10.1016/j.matpr.2021.04.369.

[25] P. Tamburrano, P. De Palma, A.R. Plummer, E. Distaso, R. Amirante, Simulink Modelling For Simulating Intensive Care Mechanical Ventilators, E3S Web Conf. 197 (2020) 07007. https://doi.org/10.1051/e3sconf/202019707007.

[26] P. Tamburrano, F. Sciatti, E. Distaso, L. Di Lorenzo, R. Amirante, Validation of a Simulink Model for Simulating the Two Typical Controlled Ventilation Modes of Intensive Care Units Mechanical Ventilators, Appl. Sci. 12 (2022) 2057. https://doi.org/10.3390/app12042057.

[27] B. Diong, J. Grainger, M. Goldman, H. Nazeran, A comparison of linear respiratory system models based on parameter estimates from PRN forced oscillation data, in: 2009 Annu. Int. Conf. IEEE Eng. Med. Biol. Soc., IEEE, Minneapolis, MN, 2009: pp. 2879–2882. https://doi.org/10.1109/IEMBS.2009.5333109.

[28] T. Woo, B. Diong, L. Mansfield, M. Goldman, P. Nava, H. Nazeran, A Comparison of Various Respiratory System Models Based on Parameter Estimates From Impulse Oscillometry Data, in: 26th Annu. Int. Conf. IEEE Eng. Med. Biol. Soc., IEEE, San Francisco, CA, USA, 2004: pp. 3828–3831. https://doi.org/10.1109/IEMBS.2004.1404072.

[29] S. Baswa, H. Nazeran, P. Nava, B. Diong, M. Goldman, Evaluation of Respiratory System Models Based on Parameter Estimates from Impulse Oscillometry Data, in: 2005 IEEE Eng. Med. Biol. 27th Annu. Conf., IEEE, Shanghai, China, 2005: pp. 2958–2961. https://doi.org/10.1109/IEMBS.2005.1617094.

[30] E. Saatci, E. Saatci, A. Akan, Analysis of linear lung models based on state-space models, Comput. Methods Programs Biomed. 183 (2020) 105094. https://doi.org/10.1016/j.cmpb.2019.105094.

[31] S.M. Maggiore, J.-C. Richard, L. Brochard, What has been learnt from P/V curves in patients with acute lung injury/acute respiratory distress syndrome, Eur. Respir. J. 22 (2003) 22s–26s. https://doi.org/10.1183/09031936.03.00004204.

[32] J.G. Venegas, R.S. Harris, B.A. Simon, A comprehensive equation for the pulmonary pressure-volume curve, J. Appl. Physiol. 84 (1998) 389–395. https://doi.org/10.1152/jappl.1998.84.1.389.

[33] J. Masip, A. Mas, Noninvasive ventilation in acute respiratory failure, Int. J. Chron. Obstruct. Pulmon. Dis. (2014) 837. https://doi.org/10.2147/COPD.S42664.

[34] O. Linares-Perdomo, T.D. East, R. Brower, A.H. Morris, Standardizing Predicted Body Weight Equations for Mechanical Ventilation Tidal Volume Settings, (n.d.).

[35] J.X. Brunner, G. Wolff, Pulmonary Function Indices in Critical Care Patients, Springer Berlin Heidelberg, Berlin, Heidelberg, 1988. https://doi.org/10.1007/978-3-642-73040-5.

[36] J.-M. Arnal, A. Garnero, M. Saoli, R.L. Chatburn, Parameters for Simulation of Adult Subjects During Mechanical Ventilation, Respir. Care 63 (2018) 158–168. https://doi.org/10.4187/respcare.05775.

[37] R.S. Harris, Pressure-Volume Curves of the Respiratory System, Respir. CARE 50 (2005).

[38] G. Servillo, E. De Robertis, S. Maggiore, F. Lemaire, L. Brochard, R. Tufano, The upper inflection point of the pressure-volume curve: Influence of methodology and of different modes of ventilation, Intensive Care Med. 28 (2002) 842–849. https://doi.org/10.1007/s00134-002-1293-7.

[39] I.G. Bikker, J. Van Bommel, D. Miranda, J. Bakker, D. Gommers, End-expiratory lung volume during mechanical ventilation: a comparison with reference values and the effect of positive end-expiratory pressure in intensive care unit patients with different lung conditions, Crit. Care 12 (2008) R145. https://doi.org/10.1186/cc7125.

[40] J. Ibañez, J.M. Raurich, Normal values of functional residual capacity in the sitting and supine positions, Intensive Care Med. 8 (1982) 173–177. https://doi.org/10.1007/BF01725734.

[41] H. Aguirre-Bermeo, M. Turella, M. Bitondo, J. Grandjean, S. Italiano, O. Festa, I. Morán, J. Mancebo, Lung volumes and lung volume recruitment in ARDS: a comparison between supine and prone position, Ann. Intensive Care 8 (2018) 25. https://doi.org/10.1186/s13613-018-0371-0.

[42] G. Natalini, D. Tuzzo, A. Rosano, M. Testa, M. Grazioli, V. Pennestrì, G. Amodeo, P.F. Marsilia, A. Tinnirello, F. Berruto, M. Fiorillo, M. Filippini, A. Peratoner, C. Minelli, A. Bernardini, Assessment of Factors Related to Auto-PEEP, Respir. Care 61 (2016) 134–141. https://doi.org/10.4187/respcare.04063.

[43] S.B. Montesi, J.P. Bakker, M. Macdonald, L. Hueser, S. Pittman, D.P. White, A. Malhotra, Air Leak during CPAP Titration as a Risk Factor for Central Apnea, J. Clin. Sleep Med. 09 (2013) 1187–1191. https://doi.org/10.5664/jcsm.3166.

[44] L.S. Menga, L. Delle Cese, T. Rosà, M. Cesarano, R. Scarascia, T. Michi, D.G. Biasucci, E. Ruggiero, A.M. Dell'Anna, S.L. Cutuli, E.S. Tanzarella, G. Pintaudi, G. De Pascale, C. Sandroni, S.M. Maggiore, D.L. Grieco, M. Antonelli, Respective Effects of Helmet Pressure Support, Continuous Positive Airway Pressure, and Nasal High-Flow in Hypoxemic Respiratory Failure: A Randomized Crossover Clinical Trial, Am. J. Respir. Crit. Care Med. 207 (2023) 1310–1323. https://doi.org/10.1164/rccm.202204-0629OC.

[45] A. Mocellin, F. Guidotti, S. Rizzato, M. Tacconi, G. Bruzzi, J. Messina, D. Puggioni, A. Patsoura, R. Fantini, L. Tabbì, I. Castaniere, A. Marchioni, E. Clini, R. Tonelli, Monitoring and modulation of respiratory drive in patients with acute hypoxemic respiratory failure in spontaneous breathing, Intern. Emerg. Med. 19 (2024) 2105–2119. https://doi.org/10.1007/s11739-024-03715-3.

[46] G. Bellani, S. Isgrò, R. Fumagalli, Helmet Continuous Positive Airway Pressure: Theory and Technology, in: A.M. Esquinas (Ed.), Noninvasive Mech. Vent., Springer Berlin Heidelberg, Berlin, Heidelberg, 2010: pp. 7–12. https://doi.org/10.1007/978-3-642-11365-9_2.

[47] C.J. Roth, T. Becher, I. Frerichs, N. Weiler, W.A. Wall, Coupling of EIT with computational lung modeling for predicting patient-specific ventilatory responses, J. Appl. Physiol. 122 (2017) 855–867. https://doi.org/10.1152/japplphysiol.00236.2016.

[48] S. Neelakantan, T. Mukherjee, K. Myers, R. Rizi, R. Avazmohammadi, Physics-informed motion registration of lung parenchyma across static CT images, in: 2024 46th Annu. Int. Conf. IEEE Eng. Med. Biol. Soc. EMBC, IEEE, Orlando, FL, USA, 2024: pp. 1–4. https://doi.org/10.1109/EMBC53108.2024.10781530.

[49] S. Neelakantan, T. Mukherjee, B.J. Smith, K. Myers, R.R. Rizi, R. Avazmohammadi, In-silico CT lung phantom generated from finite-element mesh, in: M.E. Rettmann, J.H. Siewerdsen (Eds.), Med. Imaging 2024 Image-Guid. Proced. Robot. Interv. Model., SPIE, San Diego, United States, 2024: p. 80. https://doi.org/10.1117/12.3006973.

[50] S. Neelakantan, Y. Xin, D.P. Gaver, M. Cereda, R. Rizi, B.J. Smith, R. Avazmohammadi, Computational lung modelling in respiratory medicine, J. R. Soc. Interface 19 (2022) 20220062. https://doi.org/10.1098/rsif.2022.0062.

[51] C. M. Geitner, L. J. Köglmeier, I. Frerichs, P. Langguth, M. Lindner, D Schädler, N. Weiler, T. Becher, W. A. Wall, Pressure- and time-dependent alveolar recruitment derecruitment in a spatially resolved patient-specific computational model for injured human lungs, Numer Methods Biomed Eng (2023).

[52] M. Cabeleira, D. Anand, S. Ray, C. Black, N. Ovenden, V. Diaz-Zuccarini, Comparing physiological impacts of positive pressure ventilation versus self-breathing via a versatile cardiopulmonary model incorporating a novel alveoli opening mechanism.

[53] L. D'Orsi, G. Pósfai, A. De Gaetano, A Model of the Maldistribution of Ventilation and Perfusion, in the Lungs of Heart Failure Patients, Acta Polytech. Hung. 21 (2024) 147–158. https://doi.org/10.12700/APH.21.9.2024.9.10.

[54] A. Deyranlou, A. Revell, A. Keshmiri, A Coupled Flow-Thermoregulation Lumped Model to Investigate Cardiac Function, (2021). https://doi.org/10.1101/2021.05.02.442367.

[55] C. Ngo, S. Dahlmanns, T. Vollmer, B. Misgeld, S. Leonhardt, An object-oriented computational model to study cardiopulmonary hemodynamic interactions in humans, Comput. Methods Programs Biomed. 159 (2018) 167–183. https://doi.org/10.1016/j.cmpb.2018.03.008.

[56] A. Tonini, C. Vergara, F. Regazzoni, L. Dede', R. Scrofani, C. Cogliati, A. Quarteroni, A mathematical model to assess the effects of COVID-19 on the cardiocirculatory system, Sci. Rep. 14 (2024) 8304. https://doi.org/10.1038/s41598-024-58849-3.

[57] H. Sterzik, M. Kumpf, C.F. Poets, B. Haase, Simulated model revealed significant continuous positive airway pressure fluctuations with facemasks, Acta Paediatr. 113 (2024) 1531–1533. https://doi.org/10.1111/apa.17244.

[58] V. Sartorius, B. Loi, L. Vivalda, G. Regiroli, S. De La Rubia-Ortega, L. Pezza, M. Midevaine, S. Shankar-Aguilera, R. Ben-Ammar, D. De Luca, Effect of different CPAP levels on ultrasound-assessed lung aeration and gas exchange in neonates, Respir. Res. 25 (2024) 375. https://doi.org/10.1186/s12931-024-03010-x.

[59] V. Gruber, M.B. Tracy, M.K. Hinder, S. Morakeas, M. Dronavalli, T. Drevhammar, What CPAP to use in the delivery room? Bench comparison of two methods to provide continuous positive airways pressure in neonates, BMJ Paediatr. Open 8 (2024) e002948. https://doi.org/10.1136/bmjpo-2024-002948.

[60] C.M. Ní Chathasaigh, E.A. Dunne, L.E. Geraghty, M.C. Murphy, E. O'Currain, L.K. McCarthy, C.P.F. O'Donnell, Selective or routine face mask application for breathing support of preterm infants at birth: a randomised trial, Resuscitation (2024) 110467. https://doi.org/10.1016/j.resuscitation.2024.110467.

[61] J. Helms, P. Catoire, L. Abensur Vuillaume, H. Bannelier, D. Douillet, C. Dupuis, L. Federici, M. Jezequel, M. Jozwiak, K. Kuteifan, G. Labro, G. Latournerie, F. Michelet, X. Monnet, R. Persichini, F. Polge, D. Savary, A. Vromant, I. Adda, S. Hraiech, Oxygen therapy in acute hypoxemic respiratory failure: guidelines from the SRLF-SFMU consensus conference, Ann. Intensive Care 14 (2024) 140. https://doi.org/10.1186/s13613-024-01367-2.